# Modulation Strategy to Operate the Dual Active Bridge DC–DC Converter Under Soft Switching in the Whole Operating Range

Germán G. Oggier, Guillermo O. García, and Alejandro R. Oliva

*Abstract*—A new modulation strategy that allows operating the dual active bridge (DAB) dc–dc converter under soft switching in the whole operating range is proposed. This strategy is ruled by imposing a certain modulation index in one of the two bridges and a phase shift between the transformer primary and secondary voltages. Moreover, the proposed algorithm reduces the reactive power and thus reducing the converter conduction losses. An experimental prototype was implemented and some experimental results are presented to validate the theoretical analysis. The experimental results reveal that the overall efficiency of the DAB topology can be improved up to 20% by implementing the proposed modulation strategy instead of the conventional one.

*Index Terms*—DC–DC converters, dual active bridge (DAB) converter, modulation strategy, soft switching.

## I. INTRODUCTION

THE DUAL active bridge (DAB) converter was originally proposed in [1]. It is a buck and boost bidirectional dc–dc converter, isolated by a high-frequency transformer, resulting in an interesting alternative for applications where high efficiency and power density are needed [2]–[4].

Bidirectional buck and boost dc–dc converters play an important role in the implementation of power electronics interfaces for future power systems based on smart-grid technologies [5]. Interconnections between the grid and different storage systems or dc energy sources, as for instance fuel cell, batteries, ultracapacitors, or photovoltaic subsystems, can be cited as examples of these applications [6]–[9], as well as in hybrid systems and electrical and hybrid vehicles to adapt different levels of voltage and control the power flow among the different components [10], [11].

Many efforts have been made in order to minimize losses in power electronics design. They mainly consist in minimizing the circulating currents, thus minimizing conduction losses and operating the converters under soft switching to minimize switching losses [12]–[14].

The DAB topology using the conventional modulation strategy (CMS) can operate under soft switching, thus minimizing the power semiconductor switching losses, but only within a reduced range of operation, depending on the voltage conversion ratio and on the output current [4], [14], [15]. This is an important drawback for some applications that operate most of the time with variable or low load because the overall efficiency is reduced [16]–[18].

A novel dual-phase-shift control to eliminate the reactive power with the objective of minimizing the DAB converter conduction losses, is proposed in [19]. However, this proposal fails to operate the converter under soft switching over its full operation range; the operation with variable voltage conversion ratios is not analyzed.

In [17], a modulation strategy is proposed to minimize the total DAB converter losses. This strategy consists of minimizing the modeled semiconductor (conducting and switching) and the transformer (winding and magnetic core) losses. The modulation index and the phase shift between the transformer primary and secondary voltages are used as manipulated variables to minimize DAB converter total losses as functions of the required output power. Because of the way in which the minimization algorithm was formulated, only the positive values of phase shift can be considered and as a result the operating range under soft switching could not be extended to the whole operation range. Another problem of this method is that minimization depends on the model parameters, which are usually not exactly well known in practice.

In this paper, a new analysis of the operation under soft-switching mode is carried out and as a result a new modulation strategy (NMS) that allows extending the operation under soft switching into the whole operating range is proposed. In this paper, an algorithm to implement the new modulation that allows also reduce the reactive power to reduce conduction losses is proposed .

This paper is organized as follows. In Section I, an introduction is stated. Section II presents a power-flow analysis using the NMS. Section III is demonstrating that it is possible to operate the converter under soft switching in its whole operation

G. G. Oggier and G. O. García are with the Consejo Nacional de Investigaciones Científicas y Técnicas, Buenos Aires, Argentina, and also with the Grupo de Electrónica Aplicada, Facultad de Ingeniería, Universidad Nacional de Río Cuarto, Córdoba, Río Cuarto X5804BYA, Argentina (e-mail: goggier@ing.unrc.edu.ar; g.garcia@ieee.org).

A. R. Oliva is with the Consejo Nacional de Investigaciones Científicas y Técnicas, Buenos Aires C1033AAJ, Argentina, and also with the Departamento de Ingeniería Eléctrica y Computadoras, Instituto de Investigaciones en Ingeniería Eléctrica "Alfredo Desages," Universidad Nacional del Sur, Bahía Blanca, Buenos Aires 8000, Argentina (e-mail: aoliva@uns.edu.ar).

Fig. 1. DAB converter simplified scheme.

range and minimize reactive power thus minimizing conduction losses. Finally, an algorithm to implement the NMS is proposed. In Section IV are presented some experimental results. Conclusion is drawn in Section V.

## II. POWER FLOW ANALYSIS USING THE NMS

A complete analysis of the DAB converter operation using CMS can be found in [1], [20].

In order to simplify the analysis in this paper, the high-frequency transformer is represented by its leakage inductance, as it was proposed in [20], [21]. For the present analysis, the transformers turns ratio will be considered hereinafter equal to 1. Then the converter can be represented by the simplified scheme of the two bridges $B_1$ and $B_2$ connected by the transformer leakage inductance $L$, as it is shown in Fig. 1.

The CMS consists of controlling both bridges in order to generate a voltage square waveform with 50% of duty cycle. The power flow can be controlled by manipulating the phase shift $\delta$ between the voltages of the transformer terminals $v_{T1}$ and $v_{T2}$ [1].

The modulation strategy proposed in this paper consists of driving the bridge with the largest dc voltage to generate a three-level pulse width modulation (PWM) voltage waveform while the other bridge generates a constant frequency 50% duty-cycle square voltage waveform. The output power is controlled by applying a certain phase shift $\delta$, either positive or negative.

Fig. 2 shows the ideal waveforms for the NMS when power flows from $V_1$ to $V_2$ according the variables shown in Fig. 1. For all cases shown in Fig. 2, $\delta$ is the phase shift between $v_{T1}$ and $v_{T2}$, $\beta$ corresponds to the zero crossing of the current $i_L$, $\alpha$ is the angle at which $i_L$ reaches its maximum value, and $\tau$ is the width of the pulse generated by the bridge fed with the largest dc voltage ($\tau = \pi$ for the CMS).

Fig. 2(a) and (b) shows the ideal waveforms corresponding to the DAB converter operating with the NMS when $V_1 > V_2$ (buck mode), therefore, bridge $B_1$ is driving to modulate $v_{T1}$ for two particular cases: $\delta \geq 0°$ and $\delta < 0°$, respectively.

Fig. 2(c) and (d) shows similar information but for the DAB converter operating with the NMS when $V_1 < V_2$ (boost mode), therefore, $B_2$ is driving to modulate $v_{T2}$.

All the cases shown in Fig. 2 correspond to the DAB converter operating under zero voltage switching soft-switching mode [22] and they are used to determine the DAB converter soft-switching constraints when it operates with the NMS.

The DAB converter average output power can be obtained, for both buck and boost operating modes by solving the following expression:

$$P_0 = \frac{1}{\pi} \int_0^\pi v_{T1}(\theta)\, i_L(\theta) d\theta \qquad (1)$$

where

$$v_{T1}(\theta) = \begin{cases} V_1; \text{ for } (0 < \theta < \alpha) & \text{if } (d < 1) \\ V_1; \text{ for } (0 < \theta < \pi) & \text{if } (d > 1) \end{cases} \qquad (2)$$

$\theta = \omega t$, $\omega = 2\pi f_s$, $f_s$ is the switching frequency; $\alpha = \tau$ and $\alpha = \pi - \tau + \delta$, for buck and boost operation modes, respectively, and $d$ is defined as the DAB voltage conversion ratio, $V_2/V_1$. The expressions for $i_L(\theta)$ corresponding to the different intervals and operation modes, defined in Fig. 2, are shown in Table I.

By solving (1), the following expressions can be obtained as a function of the feeding voltage, $V_1$, for $\delta \geq 0°$:

$$P_0 = \frac{V_1^2 d(2\delta m\pi - 2\delta^2 - (m\pi)^2 + m\pi^2)}{2\omega L\pi} \qquad (3)$$

and for $\delta < 0$

$$P_0 = \frac{V_1^2 dm(\pi + 2\delta - m\pi)}{2\omega L} \qquad (4)$$

where $m$ is the modulation index of the corresponding bridge, defined as $m = \tau/\pi$ [21].

Equations (3) and (4) are valid for both buck and boost operation modes.

It can be deduced from (3) and (4) that the output power can be controlled by manipulating both variables: $\delta$ and $m$.

From (3) and (4), it can be determining the following expression to calculate $\delta$ in function of the power flow to be transferred as follows:

For $\delta \geq 0°$

$$\delta = \frac{m\pi}{2} - \frac{\sqrt{(2(V_1 d\pi)^2 m - (V_1 d\pi m)^2 - 4P_0 d\omega L\pi)}}{2V_1 d}. \qquad (5)$$

For $\delta < 0°$

$$\delta = \frac{dm\pi V_1^2(m-1) + 2P_0\omega L}{2dmV_1^2}. \qquad (6)$$

In order to determine the maximum value of power that can be transferred for each value of $m$ and $\delta$, the derivative of (3) with respect to $\delta$ must be equaled zero, yielding

$$\frac{\partial P_0}{\partial \delta} = 0 = \frac{V_1^2 d(m\pi - 2\delta)}{\omega L\pi}. \qquad (7)$$

The values of $\delta$ associated to the maximum values of power for each $m$ can be obtained from (7), yielding

$$\delta = \frac{1}{2}m\pi. \qquad (8)$$

| Intervals | 1 | 2 | 3 | 4 | 5 | 6 | 7 | 8 |
|---|---|---|---|---|---|---|---|---|
| Particular Angles | 0 | β | δ | α | π | | | 2π |
| Conducting switches | $D_{12}$ $D_{13}$ $D_{22}$ $D_{23}$ | $T_{12}$ $T_{13}$ $T_{22}$ $T_{23}$ | $T_{12}$ $T_{13}$ $D_{21}$ $D_{24}$ | $D_{11}$ $D_{14}$ $D_{21}$ $D_{24}$ | $D_{11}$ $D_{14}$ $D_{21}$ $D_{24}$ | $T_{11}$ $T_{14}$ $T_{21}$ $T_{24}$ | $T_{11}$ $T_{14}$ $T_{22}$ $D_{23}$ | $D_{12}$ $T_{14}$ $D_{22}$ $D_{23}$ |

(a)

| Intervals | 1 | 2 | 3 | 4 | 5 | 6 |
|---|---|---|---|---|---|---|
| Particular Angles | 0 | $β_1$ | α | $β_2$ | $(π+δ)$ | π |
| Conducting switches | $D_{12}$ $D_{13}$ $T_{21}$ $T_{24}$ | $T_{12}$ $T_{13}$ $D_{21}$ $D_{24}$ | $D_{11}$ $T_{13}$ $D_{21}$ $D_{24}$ | $T_{11}$ $D_{13}$ $T_{21}$ $T_{24}$ | $T_{11}$ $D_{13}$ $T_{22}$ $D_{23}$ | $D_{11}$ $T_{13}$ $D_{22}$ $T_{23}$ |

(b)



| Intervals | 1 | 2 | 3 | 4 | 5 | 6 | 7 | 8 |
|---|---|---|---|---|---|---|---|---|
| Particular Angles | 0 | β | δ | α | π | | | 2π |
| Conducting switches | $D_{12}$ $D_{13}$ $D_{22}$ $D_{23}$ | $T_{12}$ $T_{13}$ $T_{22}$ $T_{23}$ | $T_{12}$ $T_{13}$ $T_{22}$ $D_{24}$ | $T_{11}$ $T_{13}$ $D_{21}$ $D_{24}$ | $D_{11}$ $D_{14}$ $D_{21}$ $D_{24}$ | $T_{11}$ $T_{14}$ $T_{21}$ $T_{24}$ | $T_{11}$ $T_{14}$ $T_{21}$ $D_{23}$ | $T_{11}$ $T_{14}$ $D_{22}$ $D_{23}$ |

(c)

| Intervals | 1 | 2 | 3 | 4 | 5 | 6 |
|---|---|---|---|---|---|---|
| Particular Angles | α | $β_1$ | $(π+δ)$ | $β_2$ | π | |
| Conducting switches | $T_{11}$ $T_{14}$ $D_{21}$ $D_{24}$ | $D_{11}$ $D_{14}$ $T_{21}$ $T_{24}$ | $D_{11}$ $D_{14}$ $D_{22}$ $T_{24}$ | $T_{11}$ $T_{14}$ $T_{22}$ $T_{24}$ | $D_{12}$ $D_{13}$ $T_{22}$ $D_{24}$ | $T_{12}$ $T_{13}$ $D_{22}$ $T_{24}$ |

(d)

Fig. 2. Ideal voltages and current waveforms using the NMS: (a) buck mode for $δ ≥ 0°$; (b) buck mode for $δ < 0°$; (c) boost mode for $δ ≥ 0°$; and (d) boost mode for $δ < 0°$.

The maximum output value as a function of $m$ can be obtained by replacing (8) in (3), yielding

$$P_{0\max} = \frac{V_1^2 d\pi m(2-m)}{4\omega L}. \tag{9}$$

Equation (8) also allows determining the minimum value of $m$ that can be applied to reach a desired output power. For this to be achieved, (8) is replaced in (3) and then the resulting equation is solved for $m$, yielding

$$m_{\min} = 1 - \frac{\sqrt{((V_1 d\pi)^2 - 4dP_0\omega L\pi)}}{V_1 d\pi}. \tag{10}$$

Based on the analysis presented in this section, an algorithm to determine the values of $δ$ and $m$ as functions of the con-

verter operation point to implement the NMS is proposed in the Section III.

## III. ALGORITHM TO IMPLEMENT THE NMS

Section III-A contains an analysis of the restriction of the DAB converter operation under soft switching, demonstrating that it is possible to operate the converter under soft switching in its whole operation range through adequately manipulating variables $δ$ and $m$.

Section III-B analyzes the reactive power minimization in order to reduce it and consequently reduce the conduction losses.

Finally, Section III-C proposes a modulation algorithm to operate the DAB converter under soft switching in the whole operation range and minimize the reactive power.

TABLE I
EXPRESSIONS TO REPRESENT $i_L$ FOR EACH INTERVAL AND OPERATING MODE DEFINED IN FIG. 2

| $\delta \geq 0$ | Intervals 1 and 2 $(0 < \theta < \delta)$ | Intervals 3 $(\delta < \theta < \alpha)$ | Intervals 4 $(\alpha < \theta < \pi)$ |
|---|---|---|---|
| Buck | $i_L(\theta) = \dfrac{(V_1 + V_2)}{\omega L}\theta + i_L(0)$ | $i_L(\theta) = \dfrac{(V_1 - V_2)}{\omega L}(\theta - \delta) + i_L(\delta)$ | $i_L(\theta) = \dfrac{-V_2}{\omega L}(\theta - \alpha) + i_L(\alpha)$ |
| Boost | $i_L(\theta) = \dfrac{(V_1 + V_2)}{\omega L}\theta + i_L(0)$ | $i_L(\theta) = \dfrac{V_1}{\omega L}(\theta - \delta) + i_L(\delta)$ | $i_L(\theta) = \dfrac{(V_1 - V_2)}{\omega L}(\theta - \alpha) + i_L(\alpha)$ |
| $\delta < 0$ | Intervals 1 and 2 $(0 < \theta < \alpha)$ | Intervals 3 $(\alpha < \theta < \pi + \delta)$ | Intervals 4 $(\pi + \delta < \theta < \pi)$ |
| Buck | $i_L(\theta) = \dfrac{(V_1 - V_2)}{\omega L}\theta + i_L(0)$ | $i_L(\theta) = \dfrac{(-V_2)}{\omega L}(\theta - \alpha) + i_L(\alpha)$ | $i_L(\theta) = \dfrac{(V_2)}{\omega L}(\theta - (\pi + \delta)) +$ $+ i_L(\pi + \delta)$ |
| Boost | $i_L(\theta) = \dfrac{(V_1)}{\omega L}\theta + i_L(0)$ | $i_L(\theta) = \dfrac{(V_1 - V_2)}{\omega L}(\theta - \alpha) + i_L(\alpha)$ | $i_L(\theta) = \dfrac{(V_1)}{\omega L}(\theta - (\pi + \delta)) +$ $+ i_L(\pi + \delta)$ |

TABLE II
SOFT-SWITCHING RESTRICTIONS

| Condition | | Buck | Boost |
|---|---|---|---|
| $\delta \geq 0$ | $i_L(\delta) \geq 0$ | $\delta \geq \dfrac{\pi(m-d)}{2}$ | $\delta \geq \dfrac{\pi(1-dm)}{2}$ |
| | $i_L(\pi) \geq 0$ | $\delta \geq \dfrac{\pi(d-m)}{2d}$ | $\delta \geq \dfrac{\pi(dm-1)}{2d}$ |
| $\delta < 0$ | $i_L(|\delta|) \geq 0$ | $m \leq d$ | $\delta < \dfrac{\pi(dm-1)}{2}$ |
| | $i_L(\pi) \geq 0$ | $\delta < \dfrac{\pi(m-d)}{2d}$ | $m \leq \dfrac{1}{d}$ |



Fig. 3. Output power versus $\delta$ and $m$ as parameter for the particular case $d = 0.4$.

## A. Soft-Switching Restrictions

The following inequalities must be fulfilled for the converter operates under soft switching [20], [21]:

$$i_L(|\delta|) > 0 \tag{11}$$

and

$$i_L(\pi) > 0. \tag{12}$$

Inequalities (11) and (12) determines the soft-switching operation limits for bridges $B_2$ and $B_1$, respectively [1], [21].

Evaluating (11) and (12) using expressions in Table I, the restrictions shown in Table II can be obtained for both bridges and both operation modes. These restrictions determine the values of $\delta$ as a function of $d$ and $m$, and allow determining the range of the output power for which the DAB converter can operate under soft switching.

Fig. 3 shows the output power as a function of $\delta$ and $m$ as parameter, for the particular case $d = 0.4$. The output power was normalized according to the base output power, $V_1^2/(\omega L)$, as it was proposed in [1]. The output power values able to be transferred under soft switching are shown in continuous line,

according to the restrictions given in Table II, whereas those under hard switching are shown in dotted line.

Fig. 3 suggests the possibility to manipulate variables $\delta$ and $m$ as a function of the output power and the voltage-conversion ratio in order to operate the DAB converter under soft switching in its whole operation range.

Fig. 4 shows the same nomogram proposed in [20] with the aim to compare the DAB converter under soft-switching operation using both CMS and NMS strategies. This nomogram shows the relationships between variables $d$ and $I_0$ [pu], with $R$ as parameter. The $R$-constant straight lines (dotted line) indicate the normalized load expressed as

$$R = \frac{d}{I_0 \,[\text{pu}]} \tag{13}$$

where

$$I_0[\text{pu}] = \frac{P_0}{V_1^2 d/(\omega L)} = \frac{\delta(2m\pi) - 2\delta^2 + \pi^2(m - m^2)}{2\pi}. \tag{14}$$
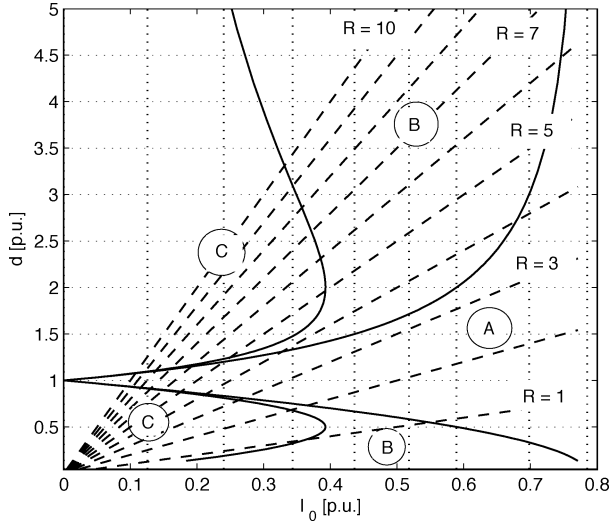
Fig. 4.  Soft-switching regions as a function of $d$ and $I_0$ [pu] with $R$ as parameter. (A)- Soft-Switching region for both modulation strategies: CMS and NMS with $\delta \geq 0$. (B)- Soft-Switching region using the NMS with $\delta \geq 0$. (C)- Soft-Switching region using the NMS with $\delta < 0$.

Fig. 4 also shows the boundaries for different soft-switching regions in continuous line according to the restrictions indicated in Table II. The area A represents the soft-switching operation region whereas B + C represents the hard-switching region when the CMS is using. Area B represents the extension of the soft-switching region using the modulation strategy proposed in [21], and area C represents the extension of the soft-switching operation region using the NMS.

Boundaries between regions A and B in Fig. 4 are obtained evaluating (14) with the restrictions in Table II with $m = 1$ and $\delta \geq 0°$. On the other hand, boundaries between regions B and C are obtained evaluating (14) with $\delta = 0°$ and $m = d$, if $d < 1$ or $m = 1/d$ if $d > 1$.

From the previous analysis, it can be concluded that choosing $\delta$ and $m$ properly, it is possible to control the power flow and operate the converter under soft switching in its whole operating range.

The parasitic capacitance of the switches and dead-band effects in the soft-switching process are important when the objective is a detailed analysis of the circuit performance [18], [19]. However, since the objective of this paper is to propose a new algorithm to implement a modulation strategy to operate the DAB dc–dc topology under soft-switching in the whole operating range, the authors do not consider necessary to include this information in this paper because of the space that would be required to do so.

## B. Reactive Power Minimization

In [19], it is shown that when using the CMS, a considerable portion of the current $i_L$ is used just to generate reactive power not contributing with the active power flow, resulting in an unnecessary electrical stress on the semiconductor switches and a lower efficiency, especially under light-load operation.
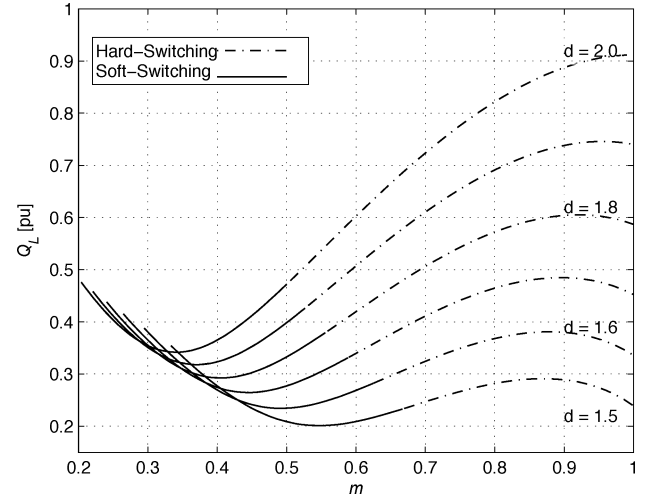


Fig. 5.  Reactive power as function of $m$ with $d$ as parameter.

In this paper, the reactive power is define as in [23] as follows:

$$Q_L = \sqrt{S_L^2 - P_L^2} \qquad (15)$$

where $P_L$ is the average instantaneous power developed in $L$, equal to zero in a switching period, and $S_L$ is the apparent power through $L$ determined as

$$S_L = V_{L\,\mathrm{rms}} I_{L\,\mathrm{rms}} \qquad (16)$$

where

$$V_{L\,\mathrm{rms}} = \sqrt{\frac{1}{\pi} \int_0^\pi (v_{T1}(\theta) - v_{T2}(\theta))^2 d\theta} \qquad (17)$$

and

$$I_{L\,\mathrm{rms}} = \sqrt{\frac{1}{\pi} \int_0^\pi (i_L(\theta))^2 d\theta}. \qquad (18)$$

Voltages $v_{T1}$ and $v_{T2}$ can be deduced from the waveforms shown in Fig. 2 to evaluate (17), while the expressions of the current $i_L$ shown in Table I can be used to evaluate (18). Table III shows the reactive power expressions according to (15) for each region and operation mode.

Fig. 5 shows the reactive power when the DAB converter operates under soft switching (solid line) and hard switching (dash-dot line), for a constant output power, as a function of $m$ and $d$ as parameter. It can be seen in this figure that the reactive power presents a minimum, which depends on $m$.

These results suggest the possibility to choose $m$ in order to minimize the reactive power when the DAB converter operates under soft switching. The possible values of $m$ that ensure the converter operation under soft-switching are bounded by a lower and an upper value, $m_l < m < m_u$ [17], where the expressions of $m_l$ and $m_u$ are shown in the Table IV.

The value of $m$ that minimizes the reactive power when the DAB converter operates under soft switching can be obtained by evaluating the expressions shown in Table III for the values $m_l < m < m_u$.

TABLE III
NORMALIZED REACTIVE POWER

| Mode | Regions | $Q_L$ [pu] |
|---|---|---|
| $d < 1$ | A+B | $\sqrt{\left(-2b\left(dm\ (1+m)\ \pi + d^3\left(3-2\ m+m^2\right)\ \pi - \left(2+2\ d^2\right)\ I_0\ [\text{pu}]\right) + d\ \pi\left(d^4\pi - 3\ d^2\left(-3+m\right)\ m\pi + m^3\pi - 12\ d\ (1+m)\ I_0\ [\text{pu}]\right)\right)/(12d)}$ |
| | C | $\sqrt{\left(m^4\pi^2 + 3d^2m^3\left(1+m\right)\pi^2 - d^3m^2\left(3+m^2\right)\pi^2 + d^4m\pi^2 + 12I_0\ [\text{pu}]^2 - 4d\left(m^4\pi^2 + 3I_0\ [\text{pu}]^2\right)\right)/(12m)}$ |
| $d > 1$ | A+B | $\sqrt{\left(d^5m^3\pi^2 + d\pi\left(-2b\left(3-2\ m+m^2\right)+\pi\right) - d^3m\pi\left(2b\left(1+m\right) + 3\left(-3+m\right)\ \pi\right) + 4bI_0\ [\text{pu}] + 4d^2\left(b - 3\left(1+m\right)\pi\right)I_0\ [\text{pu}]\right)/(12d)}$ |
| | C | $\sqrt{\left(-4d^4m^4\pi^2 + 3d^3m^3\left(1+m\right)\pi^2 - d^2m^2\left(3+m^2\right)\pi^2 - 12I_0\ [\text{pu}]^2 + d^5m^4\pi^2 + d\left(m\pi^2 + 12I_0\ [\text{pu}]^2\right)\right)/(12dm)}$ |

where $b = \sqrt{-d\pi\left(d(m-2)m\pi + 4I_0[\text{pu}]\right)}$

TABLE IV
LIMITS OF $m$ AS A FUNCTION OF $P_0$ AND $d$ FOR WHICH THE DAB CONVERTER OPERATES UNDER SOFT-SWITCHING MODE

| Region | Buck | Boost |
|---|---|---|
| A+B | $m_u = 1 - \dfrac{\sqrt{\left(V_1 d\pi\right)^2\left(1-d^2\right) - 4P_0 d\omega L\pi}}{\left(V_1 d\pi\right)}$ | $m_u = 1 - \dfrac{\sqrt{\left(V_1\pi\right)^2\left(d^2-1\right) - 4P_0 d\pi}}{\left(V_1 d\pi\right)}$ |
| | $m_l = \left(\left(V_1\pi d\right)\left(1+2d\right) + \sqrt{2\pi d\left(V_1^2\pi d^2\left(1+d\right) - 2a_1 P_0\right)}\right)/\left(V_1\pi a_1\right)$ | $m_l = \left(V_1 d\pi\left(2+d\right) + \sqrt{2\pi d}\sqrt{\pi V_1^2 d\left(1-d\right) - 2P_0 a_2}\right)/\left(V_1 d\pi a_2\right)$ |
| C | $m_u = d$ | $m_u = \dfrac{1}{d}$ |
| | $m_l = \dfrac{\sqrt{\left(1-d\right)2\pi P_0}}{\left(1-d\right)V_1\pi}$ | $m_l = \dfrac{\sqrt{\left(d-1\right)2d\pi P_0}}{\left(d-1\right)dV_1\pi}$ |

where $a_1 = 1 + 2d + 2d^2$ and $a_2 = 2 + 2d + d^2$.

Fig. 6 shows the calculated level curves for $m$ as a function of $I_0$ [pu] and $d$. Thus, the value of $m$ can be determined for each DAB converter operating point by implementing a two-input table. Modulation values shown in Fig. 6 correspond to normalized values, which are independent of the DAB converter parameters. This demonstrates the robustness to parameter variation.

### C. Proposed Algorithm

In this section, an algorithm to achieve the following objectives is proposed.
1) Control the DAB converter power flow $P_0$.
2) Operate the DAB converter under soft-switching in its whole operation range.
3) Minimize reactive power.

The algorithm requires the implementation of the following steps:
1) Inputting the required $P_0$ and $d$.
2) Solve (14) to determine the value of $I_0$ [pu].
3) Determine the modulation index $m$ that minimize the reactive power using expressions shown in Table III as a function of $I_0$ [pu] and $d$. This step can be solved by implementing a two-input table according to the nomogram shown in Fig. 6.
4) Calculate $\delta$ from (5) or (6) when the DAB converter operating point belongs to A+B or C region in Fig. 4, respectively. The DAB converter operation region can be
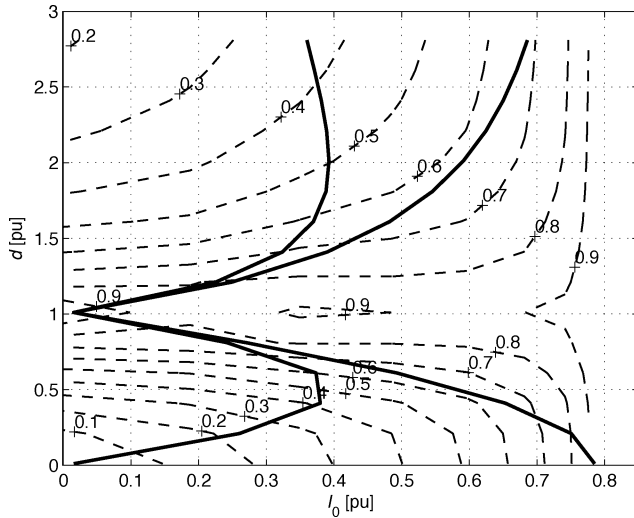
Fig. 6. Level curves showing the values of $m$ that minimize the reactive power in the plane $d$ versus $I_0$ [pu].
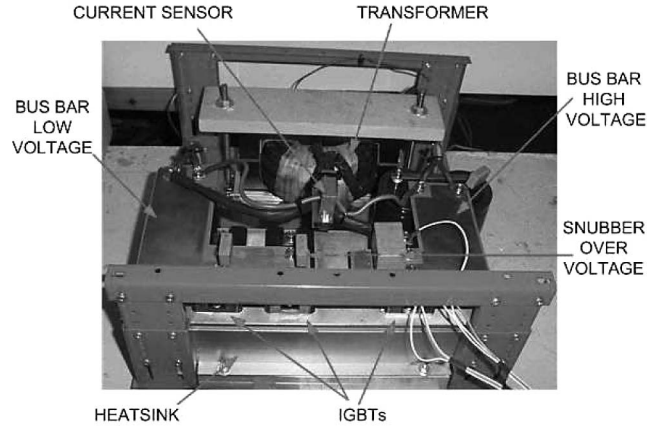


Fig. 7. Photograph of the DAB converter prototype.

TABLE V
EXPERIMENTAL PROTOTYPE CHARACTERISTICS

| | |
|---|---|
| Maximum Output Power $(P_{0\,\max})$ | 2 kW |
| Switching Frequency $(f_s)$ | 20 kHz |
| Low Voltage $(V_2)$ | 120 V |
| Voltage Conversion Ratio $(d = V_2/(nV_1))$ | 1.5 - 2.0 |
| Transformer Turns Ratio $(n)$ | 1/2.5 |
| Series Inductance $(L)$ | 20 $\mu$Hy |

determined as:

  a) if $I_0[\text{pu}] \geq I_{0,B-C}[\text{pu}]$ corresponds to region A + B;
  b) if $I_0[\text{pu}] < I_{0,B-C}[\text{pu}]$ corresponds to region
  c) where $I_{0,B-C}[\text{pu}]$ can be determined by the following expression (see Section I);

$$I_{0,B-C}[\text{pu}] = (d\pi/2)(1-d), \qquad (19)$$

for the buck mode or

$$I_{0,B-C}[\text{pu}] = (\pi/2d^2)(d-1), \qquad (20)$$

for the boost mode.

  5) Using the calculated $\delta$ and $m$, generate the modulation signals to drive the converter power switches.
  6) If $d$ or $P_0$ changes, then go back to step 1.

IV. EXPERIMENTAL RESULTS

The analysis presented in the previous sections shows that the DAB converter efficiency can be improved by using the algorithm proposed in Section III-C. To validate this proposal, a laboratory prototype to operate up to 2 kW was implemented, and experimental results were obtained. Fig. 7 shows a photograph of the actual prototype and Table V its main features. The power switches were implemented using insulated gate bipolar transistors (IGBTs) and the high-frequency transformer was built using a ferrite core and a Litz wire to reduce the conductor's losses due to the skin and the proximity effects. A digital controller to run the proposed algorithm was implemented using a DSP TMS320F2812 from Texas Instruments.

Only the results for the DAB converter operating in boost mode are presented in this section since results for operation in buck mode can be obtained similarly.

Experimental results are presented mainly to demonstrate that the efficiency of the DAB converter can be improved using the NMS instead of the CMS.

Fig. 8 shows the experimentally measured DAB converter rms current and summation of the currents at the switching angles, versus the modulation index, for two values of $I_0$ [pu]: 0.22 and 0.5, when $d = 1.5(\blacklozenge), d = 1.75$ ($\bullet$) and $d = 2.0(\blacksquare)$. In Fig. 8 are included the theoretical values (dash-dot line) determined by the expressions shown in Table I according to the definitions given in [17].

It can be observed in these figures that using $m$ according to the proposed algorithm (see Fig. 6) the currents are near the minimum value, and the conduction losses are reduced. In addition, it is evident that, for the same $I_0$, when the CMS is used ($m = 1$), the currents are larger.

Fig. 9(a)–(d) show the measured waveforms of the transformer terminal voltages and secondary current for $I_0[\text{pu}] = 0.22$ with $d = 2$ using different values of $m$. Fig. 9 shows that the DAB converter can operate under soft-switching mode when $m = 0.4$. This result agrees with the modulation index shown in Fig. 6.

Fig. 10 shows the experimentally measured efficiency versus the converter output power for three different values of the voltage-conversion ratio using both strategies. It can be concluded from these figures that the efficiency drops markedly in all cases when the output power is reduced. However, in the case of the NMS, the efficiency remains at a higher value in the whole range of the output power, becoming up to 20% higher than the achieved with the CMS for the lowest output powers.
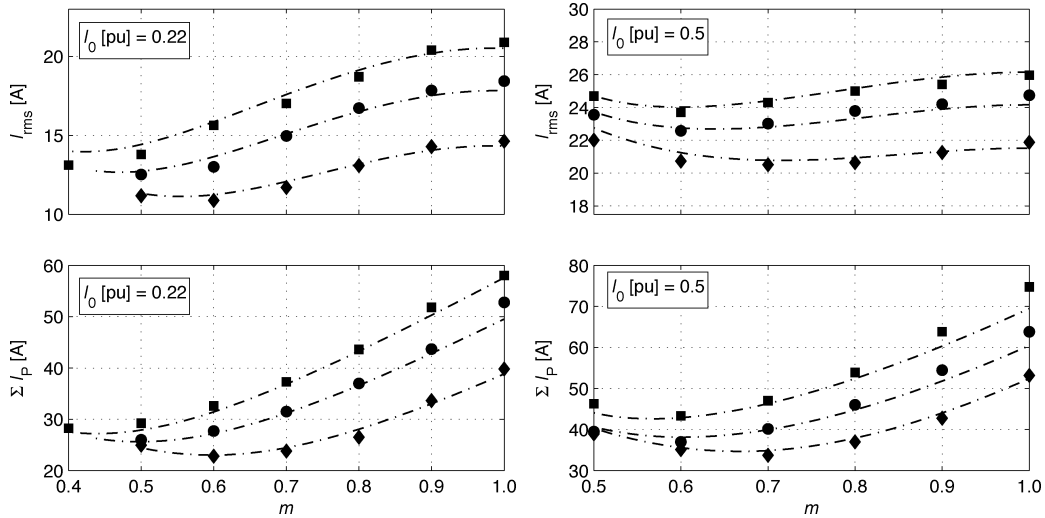
Fig. 8. Measured DAB converter rms currents (top) and summation of the currents at the switching angles (bottom) versus the modulation index $m$ $d = 1.5(\blacklozenge), d = 1.75(\bullet)$ and $d = 2.0(\blacksquare)$, and $I_0\,[\mathrm{pu}] = 0.22$ (left) and $I_0\,[\mathrm{pu}] = 0.5$ (right).
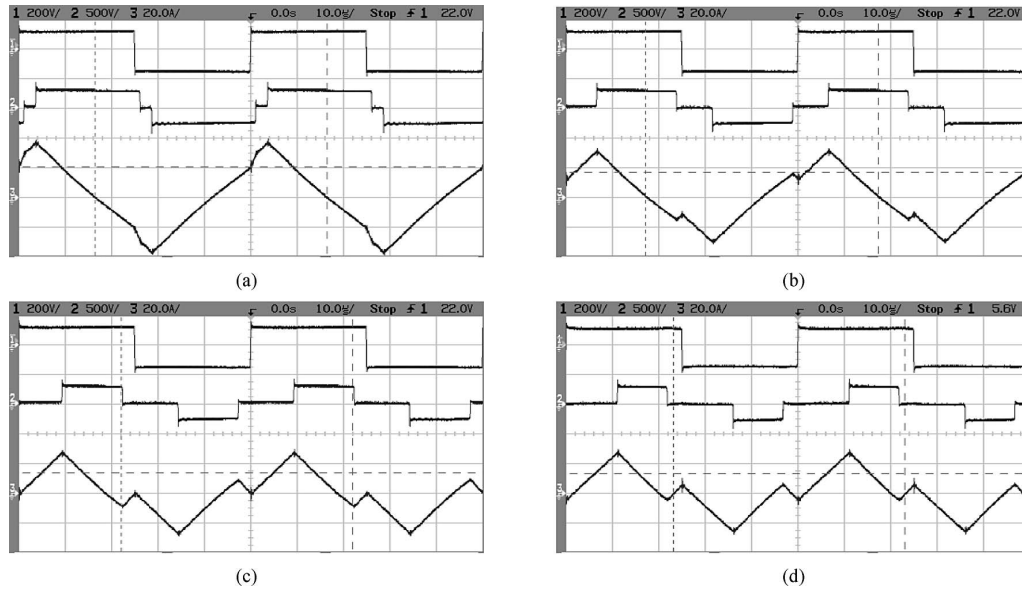


Fig. 9. Measured waveforms of transformer terminal voltages and secondary current for $d = 2.0$ and $I_0\,[\mathrm{pu}] = 0.22$: (a) $m = 0.9$; (b) $m = 0.7$; (c) $m = 0.5$; (d) $m = 0.4$.
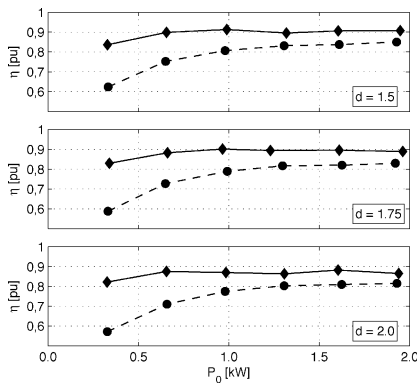


Fig. 10. Efficiency versus the DAB converter output power for both modulation strategies, ($\blacklozenge$) NMS and ($\bullet$) CMS, and three different values of voltage conversion ratio $d = 1.5$, 1.75, and 2.0.

## V. CONCLUSION

The power flow of the DAB dc–dc converter topology was analyzed and as a result an NMS was proposed. An algorithm to implement the NMS was also proposed. This algorithm allows extending the DAB topology soft-switching operation mode to its whole operation range and also allows minimizing the reactive power with the purpose to increase the overall converter efficiency.

To demonstrate the practical feasibility of the theoretical proposal, a laboratory prototype to operate up to 2 kW was implemented and some experimental results were presented.

The experimental results demonstrate that it is possible to significantly improve the efficiency of the DAB topology, especially in applications at which it operates with variable and lower power most of the time, using the proposed algorithm.

## REFERENCES

[1] R. W. De Doncker, D. M. Divan, and M. H. Kheraluwala, "A three-phase soft-switched high-power-density dc/dc converter for high-power applications," *IEEE Trans. Ind. Appl.*, vol. 27, no. 1, pp. 63–73, Jan./Feb. 1991.

[2] S. Inoue and H. Akagi, "A bidirectional isolated dc-dc converter as a core circuit of the next-generation medium-voltage power conversion system," *IEEE Trans. Power Electron.*, vol. 22, no. 2, pp. 535–542, Mar. 2007.

[3] H. Tao, A. Kotsopoulos, J. L. Duarte, and M. A. M. Hendrix, "Transformer-coupled multiport ZVS bidirectional dc-dc converter with wide input range," *IEEE Trans. Power Electron.*, vol. 23, no. 2, pp. 771–781, Mar. 2008.

[4] S. Inoue and H. Akagi, "A bidirectional dc–dc converter for an energy storage system with galvanic isolation," *IEEE Trans. Power Electron.*, vol. 22, no. 6, pp. 2299–2306, Nov. 2007.

[5] M. Liserre, T. Sauter, and J. Hung, "Future energy systems: Integrating renewable energy sources into the smart power grid through industrial electronics," *IEEE Ind. Electron. Mag.*, vol. 4, no. 1, pp. 18–37, Mar. 2010.

[6] X. Wang, F. Tian, and I. Batarseh, "High efficiency parallel post regulator for wide range input dc-dc converter," *IEEE Trans. Power Electron.*, vol. 23, no. 2, pp. 852–858, Mar. 2007.

[7] J. Biela, U. Badstuebner, and J. W. Kolar, "Impact of power density maximization on efficiency of dc-dc converter systems," *IEEE Trans. Power Electron.*, vol. 24, no. 1, pp. 288–300, Jan. 2009.

[8] N. M. L. Tan, S. Inoue, A. Kobayashi, and H. Akagi, "Voltage balancing of a 320-V, 12-F electric double-layer capacitor bank combined with a 10-kW bidirectional isolated dc-dc converter," *IEEE Trans. Power Electron.*, vol. 23, no. 6, pp. 2755–2765, Nov. 2008.

[9] M. B. Camara, H. Gualous, F. Gustin, A. Berthon, and B. Dakyo, "DC/DC converter design for supercapacitor and battery power management in hybrid vehicle applications—Polynomial control strategy," *IEEE Trans. Industrial Electron.*, vol. 57, no. 2, pp. 587–597, Feb. 2010.

[10] G.-J. Su and L. Tang, "A multiphase, modular, bidirectional, triple-voltage dc-dc converter for hybrid and fuel cell vehicle power systems," *IEEE Trans. Power Electron.*, vol. 23, no. 6, pp. 3035–3046, Nov. 2008.

[11] G.-J. Su and L. Tang, "A reduced-part, triple-voltage dc-dc converter for EV/HEV power management," *IEEE Trans. Power Electron.*, vol. 24, no. 10, pp. 2406–2410, Oct. 2009.

[12] S. Waffler and J. W. Kolar, "A novel low-loss modulation strategy for high-power bidirectional buck+ boost converters," *IEEE Trans. Power Electron.*, vol. 24, no. 6, pp. 1589–1599, Jun. 2009.

[13] M. Borage, S. Tiwari, S. Bhardwaj, and S. Kotaiah, "A full-bridge dc-dc converter with zero-voltage-switching over the entire conversion range," *IEEE Trans. Power Electron.*, vol. 23, no. 4, pp. 1743–1750, Jul. 2008.

[14] F. Krismer and J. W Kolar, "Accurate power loss model derivation of a high-current dual active bridge converter for an automotive application," *IEEE Trans. Ind. Electron.*, vol. 57, no. 3, pp. 881–891, Mar. 2010.

[15] H. Tao, J. L. Duarte, and M. A. Hendrix, "Three-port triple-half-bridge bidirectional converter with zero-voltage switching," *IEEE Trans. Power Electron.*, vol. 23, no. 2, pp. 782–792, Mar. 2008.

[16] J. Zhang, J. S. Lai, R. Y. Kim, and W. Yu, "High-power density design of a soft-switching high-power bidirectional dc–dc converter," *IEEE Trans. Power Electron.*, vol. 22, no. 4, pp. 1145–1153, Jul. 2007.

[17] G. G. Oggier, G. O. García, and A. R. Oliva, "Switching control strategy to minimize dual active bridge converter losses," *IEEE Trans. Power Electron.*, vol. 24, no. 7, pp. 1826–1838, Jul. 2009.

[18] Y. Xie, J. Sun, and J. S. Freudenberg, "Power flow characterization of a bidirectional galvanically isolated high-power DC/DC converter over a wide operating range," *IEEE Trans. Power Electron.*, vol. 25, no. 1, pp. 54–66, Jan. 2010.

[19] H. Bai and C. Mi, "Eliminate reactive power and increase system efficiency of isolated bidirectional dual-active-bridge dc-dc converter using novel dual-phase-shift control," *IEEE Trans. Power Electron.*, vol. 23, no. 6, pp. 2905–2914, Jun. 2008.

[20] M. H. Kheraluwala, R. W. Gascoigne, D. M. Divan, and E. D. Baumann, "Performance characterization of a high-power dual active bridge dc-to-dc converter," *IEEE Trans. Ind. Appl.*, vol. 28, no. 6, pp. 1294–1301, Nov./Dec. 1992.

[21] G. G. Oggier, R. Leidhold, G. O. García, A. R. Oliva, J. C. Balda, and F. Barlow, "Extending the ZVS operating range of dual active bridge high-power dc-dc converters," in *Proc. IEEE Power Electron. Spec. Conf. (PESC)*, 2006, pp. 2471–2477.

[22] M. D. Bella, T. S. Wu, A. Tchamdjou, J. Mahdavi, and M. Ehsani, "A review of soft-switched dc-ac converters," *IEEE Trans. Ind. Appl.*, vol. 34, no. 4, pp. 847–860, Jul./Aug. 1998.

[23] H. Akagi, E. H. Watanabe, and M. Aredes, *Instantaneous Power Theory and Applications to Power Conditioning*. New York: IEEE Press/Wiley Interscience, 2007, p. 30.

**Germán G. Oggier** received the degree in electrical engineering in 2003 and the M.Sc. degree in electrical engineering in 2006 from the Universidad Nacional de Río Cuarto, Río Cuarto, Argentina, and the doctorate degree in control systems from the Universidad Nacional del Sur, Argentina, in 2009.

From 1999, he joined the Grupo de Electrónica Aplicada, Universidad Nacional de Río Cuarto. He is also with the Consejo Nacional de Investigaciones Científicas y Técnicas, Buenos Aires, Argentina. His current research interests include power electronics, electric vehicles, and renewable energy conversion.

**Guillermo O. García** (M'86–S'90–SM'01) received the degree in electrical and electronics engineering from the National University of Cordoba, Cordoba, Argentina, in 1981, and the M.Sc. and Ph.D. degrees in electrical engineering from COPPE, Federal University of Rio de Janeiro, Rio de Janeiro, Brazil, in 1990 and 1994, respectively.

In 1994, he joined the National University of Rio Cuarto, Rio Cuarto, Argentina, where he is currently the Director of the Applied Electronics Group, a Coordinator of a Graduate Program in electrical engineering, and a Professor in the Electrical and Electronics Department. He was engaged in several R&D projects, at universities and industries. He is also member of the National Research Council (Consejo Nacional de Investigaciones Científicas y Técnicas). His research interests include power electronics, motion control, electric vehicles renewable energy conversion, and industrial automation and control.

Dr. García is also engaged to the professional societies: the IEEE Industry Applications, Industrial Electronics, Power Electronics, Control Systems, Power Engineering and Education, and the Argentina Automatic Control Association.

**Alejandro R. Oliva** received the B.S.E.E. degree from the Universidad Nacional del Sur, Bahía Blanca, Argentina, in 1987, and the M.S.E.E. and Ph.D. degrees in electrical engineering from the University of Arkansas, Fayetteville, AR, in 1996 and 2004, respectively.

Since 1988, he has been in the Electrical Engineering Department, Universidad Nacional del Sur, Bahía Blanca, Argentina, where he has been a Professor since 1999. Since 2005, he has been a Member of Consejo Nacional de Investigaciones Científicas y Técnicas. From 1987 to 1988, he was with HIDRONOR S.A., where he was developing a database for modeling large hydraulic plants. From 1994 to 1996, he was with the University of Arkansas, where he was involved in an EPRI/CSW power quality research project. He has authored or coauthored a book and more than 50 journals and proceedings. His current research interests include power electronics and power management.